Synthesis and Optimum Luminescence of $CaWO_4$-Based Red Phosphors with Codoping of Eu^{3+} and Na^+

Yiguo Su, Liping Li, and Guangshe Li*

State Key Laboratory of Structural Chemistry, Fujian Institute of Research on the Structure of Matter, Graduate School of Chinese Academy of Sciences, Fuzhou 350002, P. R. China

Received April 2, 2008. Revised Manuscript Received July 23, 2008

Scheelite nanostructures $Ca_{1-2x}(Eu,Na)_{2x}WO_4$ ($0 < x \leq 0.135$) were prepared from 5 nm $Ca_{0.968}(Eu,Na)_{0.032}WO_4$ by hydrothermal treatment. The preparation of 5 nm $Ca_{0.968}(Eu,Na)_{0.032}WO_4$ at room temperature and subsequent hydrothermal treatment allow control over chemical compositions and particle size of $CaWO_4$-based red phosphors that has not yet possible when using traditional preparation methods. By careful structural and electronic characterization, it is shown that simultaneous substitutions of Eu^{3+} and Na^+ at Ca^{2+} sites were possible using this methodology, which allows one to vary the local symmetry surrounding Eu^{3+} and moreover the energy transfer from O^{2-} to Eu^{3+} and tungstate groups to Eu^{3+} for optimum luminescence. As a consequence, the obtained $CaWO_4$-based nanocrystals displayed excellent luminescence properties as demonstrated by luminescence lifetimes of milliseconds, abnormally narrowed emissions, and maximum quantum efficiencies of 92%. The results reported in this work show that it is possible to control chemical composition of oxide nanostructures for structural decoration and luminescence property tailoring via codoping aliovalent ions.

Introduction

Inorganic luminescence materials have practical applications in almost all devices for artificial light production. Rare-earth-doped nanocrystals have emerged as a new class of luminescence materials, showing merits of high stability, brightness, and flexible industrial processing ability that are suitable for lighting and display devices; transparent luminescence layers or markers on metal, ceramics, or plastics; and biolabels.[1] Particular attention has focused on the engineering of Eu^{3+}-doped nanocrystals, because the relevant red emission is a key component of the tricolor luminescence. Eu^{3+} often acts as a very efficient activator in many insulators, such as Ln_2O_3 (Ln = Y, Gd), YVO_4, and YBO_3 systems[2] for high quantum luminescence emission. From the viewpoint of the unprecedented practical applications, it is necessary to explore novel Eu^{3+}-doped red luminescent materials, because in many cases, the quantum efficiency for red emission is still limited. For instance, Wilkinson and co-workers prepared a series of Eu^{3+} complexes on the macrocyclic azacarboxylate structure that gave a quantum efficiency of 5.2%.[3] Biju et al. obtained a quantum efficiency of 18% in Eu^{3+} heterocyclic β-diketonate complexes with bidentate nitrogen donors.[4] Zhao et al. synthesized full-color mesophase silicate thin film phosphors incorporated with Eu^{3+}, which gave a quantum efficiency of up to 28.8%.[5] The limited quantum efficiencies of Eu^{3+} in these systems are of a hindrance to the possible practical applications of Eu^{3+}-doped red luminescent materials.

To obtain red luminescent materials with high quantum efficiencies, several factors, including the nature of host matrix, energy transfers, and lattice modifications, should be taken into account. It is well-known that certain host materials could be employed to photosensitize Eu^{3+} in the center of the host matrix via efficient energy transfer.[1e,6] Upon excitation, Eu^{3+} can exhibit a highly efficient and narrow emission via exchange interaction and dipole−dipole interaction for both energy migration and energy transfer from the host matrix to the luminescent center,[7] which might provide a hint on how to achieve a high quantum efficiency. For example, effective energy transfer from VO_4^{3-} to Eu^{3+} ions in bulk YVO_4:Eu^{3+} leads to a high quantum efficiency of 70%.[2c] Alkali metal ions like Li^+, Na^+, and K^+ have the chemical nature of low oxidation states and distinct ionic radii, and therefore can be used to modify the local site

* Corresponding author. E-mail: guangshe@fjirsm.ac.cn. Tel: 86-591-83702122. Fax: 86-591-83714946.

(1) (a) Dubertret, B.; Skourides, P.; Norris, D. J.; Noireaux, V.; Brivanloue, A. H.; Libchaber, A. *Science* **2002**, *298*, 1759. (b) Zhang, C. Y.; Yeh, H. C.; Kuroki, M. T.; Wang, T. H. *Nat. Mater.* **2005**, *4*, 826. (c) Wang, L.; Li, Y. D. *Chem. Commun.* **2006**, *24*, 2557. (d) Xia, H. R.; Li, L. X.; Zhang, H. J.; Meng, X. L.; Zhu, L.; Yang, Z. H.; Liu, X. S.; Wang, J. Y. *J. Appl. Phys.* **2000**, *87*, 269. (e) Yu, M.; Lin, J.; Fang, J. *Chem. Mater.* **2005**, *17*, 1783.

(2) (a) Blasse, G.; Crabmaier, B. C. *Luminescent Materials*; Springer-Verlag: New York, 1994. (b) Park, J. K.; Kim, K. N.; Bae, P. K.; Lee, J. H.; Han, C. H.; Kim, C. H. *Electrochem. Solid State Lett.* **2007**, *10*, J97. (c) Ropp, R. C. *J. Electrochem. Soc. Solid State Sci.* **1968**, *115*, 940. (d) Lin, C. K.; Kong, D. Y.; Liu, X. M.; Wang, H.; Yu, M.; Lin, J. *Inorg. Chem.* **2007**, *46*, 2674.

(3) Wilkinson, A. J.; Maffeo, D.; Beeby, A.; Foster, C. E.; Williams, J. A. G. *Inorg. Chem.* **2007**, *46*, 9438.

(4) Biju, S.; Raj, D. B. A.; Reddy, M. L. P.; Kariuki, B. M. *Inorg. Chem.* **2006**, *45*, 10651.

(5) Zhao, D.; Seo, S. J.; Bae, B. S. *Adv. Mater.* **2007**, *19*, 3473.

(6) (a) Huignard, A.; Buissette, V.; Franville, A. C.; Gacoin, T.; Boilot, J. P. *J. Phys. Chem. B* **2003**, *107*, 6754. (b) Liu, J. F.; Li, Y. D. *Adv. Mater.* **2007**, *19*, 1118. (c) Pang, M. L.; Lin, J.; Wang, S. B.; Yu, M.; Zhou, Y. H.; Han, X. M. *J. Phys.: Condens. Matter.* **2003**, *15*, 5157.

(7) (a) Hsu, C.; Powell, R. C. *Phys. Rev. Lett.* **1975**, *35*, 734. (b) Hsu, C.; Powell, R. C. *J. Lumin.* **1975**, *10*, 273. (c) Treadaway, M. J.; Powell, R. C. *Phys. Rev. B* **1975**, *11*, 862.

10.1021/cm8014435 CCC: $40.75
Published on Web 08/30/2008

symmetry of the Eu^{3+} containing materials for improving the luminescence efficiency.[8] As a self-activating phosphor, tungstate complexes have some advantages, e.g., high chemical stability, high X-ray absorption coefficient, and high average refractive index, which present efficient energy transfer from the tungstate host matrix to the localized states of the doping ions.[9] Consequently, Eu^{3+}-doped tungstate materials may serve as efficient red phosphors. It can thus be expected that Eu^{3+} ions and alkali metal ions codoped into tungstate matrix would lead to the generation of highly luminescent materials.

Calcium tungstate ($CaWO_4$) is an important member of metal tungstate families,[10] which has been generally considered as a prototype scheelite compounds with a close structural link to many materials such as $CaMoO_4$, $PbMoO_4$, $PbWO_4$, $YLiF_4$, and high-pressure phases of $TbVO_4$ and $DyVO_4$. Many methodologies[10e,11] including conventional solid-state reactions, coprecipitation, and combustion methods have been extensively studied to prepare $CaWO_4$-based nanocrystals that although attractive, still face issues in efficient control over the crystal size, morphology, and compositions that are crucial for high luminescence performance. Solution chemistry via hydrothermal routes is advantageous for homogeneous nucleation of nanocrystals with defined morphologies, nevertheless, the nucleation rate is highly sensitive to the supersaturation with respect to the relative activity of Ca^{2+} and WO_4^{2-}.[12] As a result, it is still an outstanding problem as to the simultaneous substitution of Eu^{3+} and monovalent alkali metal ions at Ca^{2+} sites of $CaWO_4$ when using solution chemistry. Having these in mind, regulation of the relative activity of reactive species (Ca^{2+}, WO_4^{2-}) by carefully choosing certain types of capping reagents[13] such as citric acid is fundamentally important, which may help to simultaneously substitute Eu^{3+} and Na^+ at Ca^{2+} sites of $CaWO_4$ for significantly improved quantum efficiency.

In this paper, we study $CaWO_4$ nanocrystals prepared in previous works[13a,b] and use multicomponent codoping of Eu^{3+} and Na^+ in $CaWO_4$ nanocrystals to show their modification to have highly luminescent properties. By using methods in this work, we show how one may control the chemical compositions and particle sizes of $CaWO_4$-based red phosphors. The simultaneous substitutions of Eu^{3+} and Na^+ at Ca^{2+} sites are demonstrated and thus the local symmetry surrounding Eu^{3+} and moreover the energy transfer from O^{2-} to Eu^{3+} and tungstate groups to Eu^{3+} can be optimized for luminescence.

Table 1. Initial Molar Ratios and Those Measured by ICP Technique for the Samples

sample	initial molar ratios Ca:Eu:W	product molar ratios Na:Ca:Eu:W	deduced product
1	0.975:0.025:1	0.042:0.968:0.016:1	$Ca_{0.968}(Eu,Na)_{0.032}WO_4$
2	0.975:0.025:1	0.087:0.942:0.029:1	$Ca_{0.942}(Eu,Na)_{0.058}WO_4$
3	0.950: 0.050:1	0.071:0.902:0.049:1	$Ca_{0.902}(Eu,Na)_{0.098}WO_4$
4	0.925:0.075:1	0.124:0.854: 0.073:1	$Ca_{0.854}(Eu,Na)_{0.146}WO_4$
5	0.900:0.100:1	0.193:0.756:0.122:1	$Ca_{0.756}(Eu,Na)_{0.244}WO_4$
6	0.850:0.150:1	0.208:0.730:0.135:1	$Ca_{0.730}(Eu,Na)_{0.270}WO_4$

Experimental Section

Analytical grade chemicals of $CaCl_2$, $Na_2WO_4 \cdot H_2O$, Eu_2O_3, citric acid, HNO_3, and NaOH were purchased from Shanghai Chemical Industrial Co. and used as the starting materials. A typical procedure for the sample synthesis is described as follows: 0.044 g of Eu_2O_3 (99.99%) was first dissolved in diluted nitrate acid on heating while stirring, and was then allowed to cool to room temperature; 1.05 g of $CaCl_2$ and 2.1 g of citric acid were added into the mixed solution while stirring. Second, 3.299 g of $Na_2WO_4 \cdot H_2O$ was slowly added to the mixed solution until a transparent solution formed. A well-controlled amount of NaOH solution was then added with magnetic stirring to pH 9 to form a white homogeneous dispersion. One portion of this suspension was sufficiently washed with distilled water and then dried at room temperature to yield sample 1. Another portion of this suspension was sealed along with the mother solution in 30 mL Teflon-lined stainless steel autoclaves and reacted at 160 °C for 12 h; sample 2 was then obtained. Using the preparation procedure for sample 2 but with varied initial molar ratios, samples 3−6 were obtained. The corresponding initial molar ratios are listed in Table 1.

Phase purities of all samples were characterized by X-ray diffraction (XRD) on Rigaku DMAX2500 X-ray diffractometer using a copper target. The average crystallite size, D, was calculated from the diffraction peak (101) using the Scherrer formula

$$D = 0.9\lambda/(\beta \cos \theta) \quad (1)$$

where λ (=1.5406 Å) is the X-ray wavelength employed, θ is the diffraction angle of the peak (101), and β is defined as the half-width after subtracting the instrumental broadening. Particle sizes and morphologies of the samples were determined using transmission electron microscopy (TEM) on a JEM-2010 apparatus with an acceleration voltage of 200 kV. The chemical compositions of the samples were measured by inductively coupled plasma (ICP) technique on a Perkin-Elmer Optima 3300DV spectrometer. Infrared spectra of the samples were recorded on a Perkin-Elmer IR spectrometer using a KBr pellet technique. Optical diffuse reflectance spectra of the samples were measured using Lambda 900 UV/vis spectrometer at room temperature. Emission and excitation

(8) (a) Yu, X. B.; Xu, X. L.; Zhou, C. L.; Tang, J. F.; Peng, X. D.; Yang, S. P *Mater. Res. Bull.* **2006**, *41*, 1578. (b) Gu, F.; Li, C. Z.; Jiang, H. B. *J. Cryst. Growth* **2006**, *289*, 400.
(9) (a) Kodaira, C.; Brito, H. F.; Felinto, M. C. F. C. *J. Solid State Chem.* **2003**, *171*, 401. (b) Jia, P. Y.; Liu, X. M.; Li, G. Z.; Yu, M.; Fang, J.; Lin, J. *Nanotechnology* **2006**, *17*, 734. (c) Lou, X. M.; Chen, D. H. *Mater. Lett.* **2008**, *62*, 1681. (d) Pang, M. L.; Lin, J.; Yu, Y. *J. Solid State Chem* **2004**, *177*, 2237. (e) Jia, P. Y.; Liu, X. M.; Yu, M.; Luo, Y.; Fang, J.; Liu, J *Chem. Phys. Lett.* **2006**, *424*, 358. (f) Dai, Q. L.; Song, H. W.; Pan, G. H.; Bai, X.; Zhang, H.; Qin, R. F.; Hu, L. Y.; Zhao, H. F.; Lu, S. Z.; Ren, X. G. *J. Appl. Phys.* **2007**, *102*, 054311. (g) Pode, R. B.; Dhoble, S. J. *Phys. Status Solidi B* **1997**, *203*, 571.
(10) (a) Pankratov, V.; Grigorjeva, L.; Millers, D.; Chernov, S.; Voloshinovskii, A. S. *J. Lumin.* **2001**, *94*, 427. (b) Park, I. H.; Kim, B. S.; Kim, K. Y.; Kim, L. H. *Jpn. J. Appl. Phys* **2001**, *40*, 4956. (c) Mogilevsky, P.; Parthasarathy, T. A.; Petry, M. D. *Acta Mater.* **2004**, *52*, 5529. (d) Kim, D. S.; Ostromecki, M.; Wachs, I. E. *J. Mol. Catal., A: Chem.* **1996**, *106*, 93. (e) Kay, M. I.; Fraizer, B. C.; Almodovar, I. J. *J. Chem. Phys.* **1964**, *40*, 504. (f) Hazen, R. M.; Finger, L. W.; Mariathasan, J. W. E. *J. Phys. Chem. Solids* **1985**, *46*, 253.
(11) (a) Chen, D.; Shen, G. Z.; Tang, K. B.; Zheng, H. G.; Qian, Y. T. *Mater. Res. Bull.* **2003**, *38*, 1783. (b) Ryu, J. H.; Yoon, J. W.; Lim, C. S.; Oh, W. C.; Shim, K. B. *Ceram. Int.* **2005**, *31*, 883. (c) Senyshyn, A.; Kraus, H.; Mikhailik, V. B.; Yakovyna, V. *Phys. Rev. B* **2004**, *70*, 214306.
(12) Pina, C. M.; Fernandez-Diaz, L.; Astilleros, J. M. *Cryst. Res. Technol.* **2000**, *35*, 1015.
(13) (a) Su, Y. G.; Li, G. S.; Xue, Y. F.; Li, L. P. *J. Phys. Chem. C* **2007**, *111*, 6684. (b) Li, L. P.; Su, Y. G.; Li, G. S. *Appl. Phys. Lett.* **2007**, *90*, 054105. (c) Lifshitz, E.; Bashouti, M.; Kloper, V.; Kigel, A.; Eisen, M. S.; Berger, S. *Nano Lett.* **2003**, *3*, 857. (d) Talapin, D. V.; Haubold, S.; Rogach, A. L.; Kornowski, A.; Haase, M.; Weller, H. *J. Phys. Chem. B* **2001**, *105*, 2260.

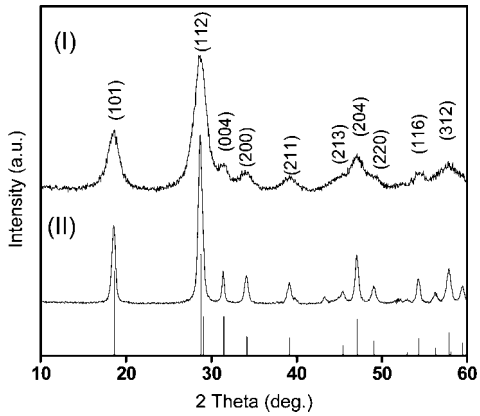

Figure 1. XRD patterns of samples 1 and 2. Vertical bars below the patterns represent the standard diffraction data for $CaWO_4$ (JCPDS card 41−1413).

spectra and transient decays of the samples were measured on an Edinburgh Instruments FLS920 spectrofluorimeter equipped with both continuous and pulsed xenon lamps.

Results and Discussion

The chemical analyses of the as-prepared samples were performed by ICP technique. As indicated in Table 1, Na, Eu, Ca, and W were detected for all samples. The final molar ratios of Ca to total metal ions in the samples were all slightly smaller than the initial ones. Increasing the initial Eu^{3+} concentration causes the Na^+ content in the final samples to increase. The concentration of Na^+ ions was larger than the concentration of Eu^{3+} ions. The presence of excess sodium in all samples may be the consequence of codoping of Eu^{3+} and Na^+ at Ca^{2+} sites and excess surface absorption of Na^+. Citric species capped on the surfaces is a likely cause for the excess surface absorption of Na^+, as it may complex with Na^+ because of charge compensation effects.

The crystallinity and phase purity of the as-prepared samples were examined with XRD. Figure 1 shows the XRD patterns of samples 1 and 2. Other samples (3−6) showed similar XRD patterns (see the Supporting Information, Figure S1). From Figure 1, it can be seen that all diffraction peaks matched well the standard data of scheelite phase $CaWO_4$ (Joint Committee for Power Diffractions Standards, JCPDS card 41−1431), and that no traces of additional peaks from other phases were observed. Therefore, all as-prepared samples were single-phase $CaWO_4$. The diffraction peaks for all samples (Figure 1) were significantly broadened, which indicates the fine nature of the particles. The average crystallite size calculated from the peak broadening of (101) line using Scherrer formula was approximately 5 nm for sample 1, which increased to about 18 nm for sample 2 after hydrothermal treatment at 160 °C. The fine nature of the samples was confirmed by TEM observations. By a least-squares method using the Retica Rietveld program (Version LHPM, 2000, B. A. Hunter and C. J. Howard, Lucas Heights Research Laboratories, Menai 2234, Australia), the cell volume for sample 1 was calculated to be 317.9 $Å^3$, which was slightly larger than that of 315.8 $Å^3$ for sample 2. The axial ratio of *c/a* increased from 2.157 for sample 1 to 2.167 for sample 2.

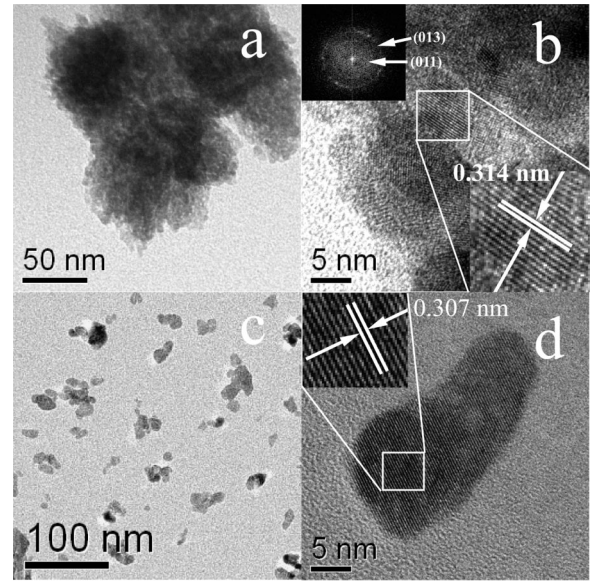

Figure 2. TEM and HRTEM images of samples 1 (a, b) and 2 (c, d) at different magnifications.

Morphological observations by TEM and HRTEM (Figure 2) indicate that sample 1 consisted of agglomerated particles and for a singular particle, the spacing between adjacent lattice fringes was 0.314 nm, which is very close to that of 0.312 nm for the (112) plane as calculated by XRD but slightly larger than that of 0.305 nm for bulk $CaWO_4$. Though sample preparation was performed at room temperature, sample 1 showed an extraordinarily high crystallinity as indicated by the ring patterns in inset of Figure 2b (i.e., fast-Fourier-transform pattern obtained from HRTEM image). The innermost ring corresponded to the (011) plane, whereas the outside one is assigned to (013) plane. Comparatively, sample 2 consisted of well dispersed nanocrystals with a spindly shape (Figures 2c,d). The diameter of the spindly particle was observed to be about 16 nm, which is close to that calculated by Scherrer formula. The interplanar spacing was about 0.307 nm (Figure 2d), which is smaller than that of the (112) plane for sample 1. Therefore, there exists a lattice expansion at smaller particle size, which is in good agreement with the XRD analysis. There are several reasons that might explain this observation. The primary reason is likely due to the structural relaxation near the surface as documented in many oxide systems like $BaTiO_3$, $PbTiO_3$, CuO, and CeO_2.[14] For the present $CaWO_4$-based nanocrystals, the surfaces are likely terminated with a large fraction of unsaturated metallic ions (e.g., Ca^{2+} or W^{6+}) that may induce a surface dipole layer. The roughly parallel surface defect dipoles at small particle sizes might produce repulsive forces that are strong enough to give negative pressure effects for the lattice expansion. It is also noted that our previous work[13b] has demonstrated that particle size reduction of $CaWO_4$ nanocrystals from 19 to 5 nm produces an increase in lattice volume by about 0.5%. For the present codoped

(14) (a) Alivisatos, A. P. *J. Phys. Chem.* **1996**, *100*, 13226. (b) Huang, T. C.; Wang, M. T.; Sheu, H. S.; Hsieh, W. F. *J. Phys.: Condens. Matter.* **2007**, *19*, 476212. (c) Ishikawa, K.; Uemori, T. *Phys. Rev. B* **1999**, *60*, 11841. (d) Palkar, V. R.; Ayyub, P.; Chattopadhyay, S.; Multani, M. *Phys. Rev. B* **1996**, *53*, 2167. (e) Zhou, X. D.; Huebner, W. *Appl. Phys. Lett.* **2001**, *79*, 3512.

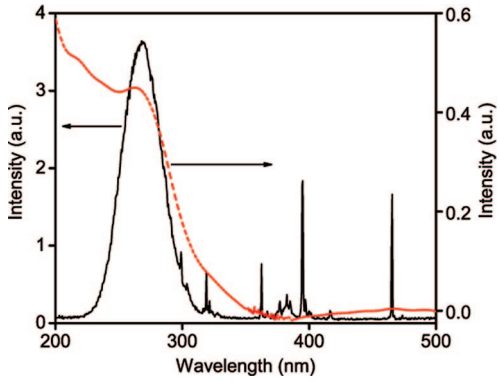

Figure 3. Optical diffuse reflectance spectrum (dash line) and excitation spectrum (solid line) of sample 2.

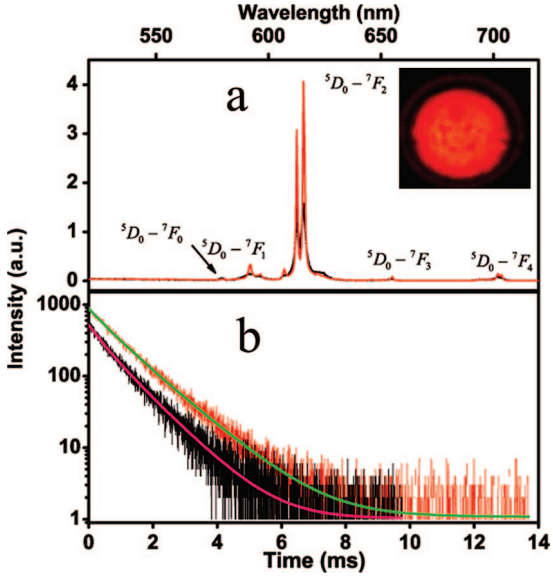

Figure 4. (a) Luminescence spectra and (b) $^5D_0$ lifetime decay curves of sample 1 (black) and sample 2 (red). Inset of (a) shows an eye-visible luminescence photo of sample 2 excited under a 365 lamp irradiation (1.5 W).

nanocrystals, the lattice volume expansion of approximately 0.66% was detected when the particle size reduced from 18 nm for sample 2 to 5 nm for sample 1. We anticipate that the excess lattice expansion of about 0.16 % may come from the doping effects as considered below. First, as Eu^{3+} substitutes in Ca^{2+} sites of $CaWO_4$, a lattice contraction is expected because the ionic radius of Eu^{3+} in 8-coordination is 1.066 Å, which is slightly smaller than that of 1.12 Å for Ca^{2+}.[15] This expectation is contrary to what we observed for our samples. Alternatively, when Na^+ partially substitutes in Ca^{2+} sites, a lattice expansion is likely to occur because of a larger ionic size of 1.18 Å for Na^+. The variation of lattice parameters for samples 2−4 as given below also confirms the codoping of Na^+ and Eu^{3+} in the $CaWO_4$ lattice.

The electronic transitions of the samples were investigated by optical diffuse reflectance spectrum. Figure 3 shows a diffuse reflectance spectrum of sample 2 in the visible region, which is characterized by a broadband peaking at 265 nm. On the basis of the literature assignments,[16] this broadband is attributed to the $^1A_1 \rightarrow {}^1T_1$ transition that originated from the charge transfer from the oxygen ligands to the central tungsten atom inside the WO_4^{2-} complex. Comparatively, the excitation spectrum of sample 2 in Figure 3 monitored at 615 nm at room temperature showed a broadband at 266 nm and some sharp lines. The sharp lines are characteristic of f−f transitions of Eu^{3+} ions,[3] which indicated that Eu ions doped in $CaWO_4$ nanocrystals are present as Eu^{3+}. In regard to the nature of the broad excitation band centered at 266 nm, there are at least two kinds of contributions to this band, namely, the charge transfer excitation of Eu^{3+} ions and the energy transition between Eu^{3+} ions and tungstate groups. The charge transfer excitation of Eu^{3+} is an electronic transition from the ground-state to the excited-state of the 4f shell, and the corresponding band position in excitation spectrum is mainly determined by the covalency of Eu−O bond and the coordination environment of Eu^{3+} as well. As usual, an increase in covalency of Eu−O bond would reduce the energy for electron transfer. In the Eu—O couple, the excitation energy for charge transfer can be estimated by the following Jorgensen's equation,[17]

$$\nu = 3[\chi(\mathrm{O}) - \chi(\mathrm{Eu})] \times 10^4 \qquad (2)$$

where ν in cm^{-1} denotes the position of the charge transfer band, χ(O) and χ(Eu) are the optical electronegativity of the oxygen and europium ions, respectively. Taking $\chi(O) = 3.2$ and $\chi(Eu) = 1.75$,[18] the band position for Eu—O charge transfer is calculated to be at 238 nm (or 42 000 cm^{-1}) which is lower than that of 250 nm reported for the charge transfer band of Eu^{3+} in $ZnWO_4$ nanocrystals.[19] Because the centered position of the broad excitation band observed for sample 2 is larger than 250 nm, it is probable that the Eu—O charge transfer contributes little to the excitation of Eu^{3+}. From Figure 3, it is also clear that the broad excitation band at 266 nm overlapped with its absorption band, as reported for cases where Eu^{3+} is doped into YVO_4 nanocrystals.[1e,6a,b,9c] Therefore, the broad excitation band in excitation spectrum should mainly originate from the energy transfer transitions from tungstate groups to Eu^{3+}.

Figure 4a shows the emission spectra of the samples under the excitation of continuous Xe-lamp irradiation. It is seen that both samples 1 and 2 showed similar emission lines but with different intensities. The electronic dipole transition of $^5D_0$—$^7F_2$ was characterized by a set of emissions at 607, 612, and 615 nm. It is noted that the most intensive emission at 615 nm is very narrow with a full width at the half-height less than 3 nm, which compares with that of approximately 19 nm reported for the 50−100 nm $CaWO_4$:Eu^{3+} incorporated in silica.[9c] The $^5D_0$—$^7F_1$ line is observed at 591 nm, which originates from the parity-allowed magnetic dipole transition. The $^5D_0$—$^7F_2$ transition is hypersensitive, while the $^5D_0$—$^7F_1$ transition is insensitive to the crystal field environment. For instance, in a site with an inversion

(15) Shannon, R. D. *Acta Crystallogr., Sect. A* **1976**, *32*, 751.
(16) Mikhailik, V. B.; Kraus, H. *J. Appl. Phys.* **2005**, *97*, 083523.
(17) Jorgensen, C. K. *Prog. Inorg. Chem.* **1970**, *12*, 101.
(18) Pieterson, L. van; Heeroma, M.; Heer, E. de; Meijerink, A. *J. Lumin.* **2000**, *91*, 177.
(19) Shigeo, S.; William, M. *Phosphor Handbook*; CRC Press: Washington, D.C., 1998.

symmetry, the magnetic dipole transition is dominant, while in a site without inversion symmetry, the $^5D_0—^7F_2$ electronic transition becomes the strongest one.[20] Therefore, the intensity ratio of the transitions $^5D_0—^7F_2$ to $^5D_0—^7F_1$,

$$R/O = I(^5D_0—^7F_2)/I(^5D_0—^7F_1) \quad (3)$$

is a good measure for the symmetry of Eu^{3+} site. The intensity of $^5D_0—^7F_2$ transition is much higher than that of $^5D_0—^7F_1$, and the R/O values calculated for samples 1 and 2 were 6.24 and 6.58, respectively, which is strong evidence that Eu^{3+} ions mainly occupy the lattice site without inversion symmetry. It is well-known that $CaWO_4$ crystallizes into a tetragonal scheelite structure with space group C_{4h}, in which Ca^{2+} is coordinated with eight oxygen atoms and has a S_4 point symmetry with no inversion center.[21] These considerations led us to assume that Eu^{3+} may be doped into the Ca^{2+} sites of the samples, in agreement with the ionic radii difference because the ionic radii of 1.066 Å for Eu^{3+} is slightly smaller than that of 1.12 Å for Ca^{2+}, but much larger than that of 0.42 Å for W^{6+} in 4-fold coordination. Nevertheless, the difference in oxidation states between Eu^{3+} and Ca^{2+} would result in the deviation of the site symmetry of Eu^{3+} from S_4 symmetry due to the charge compensation effects. Ghaderi and co-workers[22] proposed two types of charge compensating patterns, hump-shaped (type I) and flat (type II), for Eu^{3+} substitution in Ca^{2+} sites via the paths: $2Ca^{2+} = Eu^{3+} + Na^+$ for type I and $3Ca^{2+} = 2Eu^{3+} + \square$ (where $\square$ is a Ca site vacancy) for type II. Considering the proposal of Ghaderi et al.,[22] which type of charge compensation pattern could exist in the present samples? To answer this question, it is necessary to recall the lattice defects and their dependences on the long-lasting luminescence. Numerous works have investigated the long-lasting luminescence property of Eu^{2+} doped alkaline earth aluminates.[22,23] It has been concluded that the long-lasting luminescence is due to the formation of oxygen defects and cation vacancies which act as the electron or hole trapped centers.[24] These defects could be formed in a reducing atmosphere or during long-term calcinations at high temperatures that can fulfill the charge compensation effects. Long-lasting phosphorescence has been observed in Tb^{3+} activated calcium aluminate glasses[25] and in Eu^{3+}-doped alkaline earth oxide materials. Cation vacancies induced by Eu^{3+} doping in MO lattice (M = Ca, Sr, Ba) are also reported to account for the long-lasting luminescence.[26] It stands to reason that the generation of oxygen defects or cation vacancies in the lattice should yield long-lasting luminescence properties.

Here, if we supposed that the charge compensation pattern is of type II, then long-lasting luminescence behavior can be expected for both samples 1 and 2. However, from the luminescence decay curves in Figure 4b, the lifetimes of both samples 1 and 2 were calculated to be within the milliseconds, i.e., both samples did not possess long-lasting luminescence features. While in the case of the type I of charge compensation pattern, Eu^{3+} and Na^+ codoped in $CaWO_4$ lattice would lead to a charge balance and moreover a reduction in Ca^{2+} vacancy concentration. Therefore, the charge compensation pattern of the present $CaWO_4:Eu^{3+}/Na^+$ samples is most likely of the type I, since Eu^{3+} and Na^+ codoped in $CaWO_4$ matrix may induce a lattice distortion and a lowered lattice symmetry. This assumption could be verified by the presence of the very weak $^5D_0—^7F_0$ emission at 579 nm in the emission spectra since the $^5D_0—^7F_0$ emission is only allowed for C_s, C_n, C_{nv} site symmetry.[27] The deviation from S_4 symmetry for Eu^{3+} in $CaWO_4$ nanocrystals was also confirmed by the R/O value and XRD analysis as discussed below. It should be emphasized that under the excitation of continuous lights, an emission at 460 nm caused by tungstate groups was detected (see the Supporting Information, Figure S3), although the intensity was very weak. The observation of tungstate emission further confirmed the existence of energy transfer from tungstate groups to Eu^{3+} for $CaWO_4:Eu^{3+}/Na+$ nanocrystals. After being excited under a 365 lamp irradiation, both samples 1 and 2 showed red color emission, and the luminescence intensity of sample 2) was significantly enhanced (inset of Figure 4a).

The luminescence decay curves of the $^5D_0$ level in Figure 4b measured on samples 1 and 2 exhibit multiexponential feature that can be well-reproduced by a double-exponential function as

$$I = A_1\exp(-t/\tau_1) + A_2\exp(-t/\tau_2) \quad (4)$$

where τ_1 and τ_2 are the fast and slow components of the luminescent lifetimes, and A_1 and A_2 are the fitting parameters, respectively. The lifetimes for $^5D_0—^7F_2$ (615 nm, main emission) of Eu^{3+} were calculated to be $\tau_1 = 0.309$, $\tau_2 = 0.902$ ms for sample 1 and $\tau_1 = 0.636$, $\tau_2 = 1.173$ ms for sample 2, respectively. The double-exponential decay behavior of the activator is often observed when the excitation energy is transferred from the donor.[28] A very similar result has been observed in the nanocrystalline $YVO_4:Eu^{3+}$ system, where an efficient energy transfer occurs from VO_4^{3-} groups to Eu^{3+} ions.[1e] Hsu et al.[7b] proposed a model for the energy transfer and luminescence properties of $YVO_4:Eu^{3+}$ and predicted that the activator (Eu^{3+}) can exhibit a double decay curves which is consistent with our results. The average lifetimes of $^5D_0—^7F_2$ emission for Eu^{3+}, defined as[1e,28b,29]

(20) (a) Kirby, A. F.; Richardson, F. S. *J. Phys. Chem.* **1983**, *87*, 2544. (b) Stouwdam, J. W.; van Veggel, F. C. J. M. *Nano Lett.* **2002**, *2*, 733.
(21) Page, A. G.; Godbole, S. V.; Sastry, M. D. *J. Phys. Chem. Solids* **1989**, *50*, 571.
(22) Ghaderi, M.; Palin, J. M.; Campbell, I. H.; Sylvester, P. J. *Econ. Geol. Bull. Soc.* **1999**, *94*, 423.
(23) (a) Sánchez-Benítez, J.; Andrés, A. D.; Marchal, M.; Cordoncillo, E.; Regi, M. V.; Escribano, P. *J. Solid State Chem.* **2003**, *171*, 273. (b) Liu, Y. L.; Kuang, J. Y.; Lei, B. F.; Shi, C. S. *J. Mater. Chem.* **2005**, *15*, 4025. (c) Song, H. W.; Lu, S. Z.; E, S. L.; Gao, R. X.; Zhang, J. H.; Chen, B. J.; Xia, H. P.; Zhang, J. L.; Ni, Q. H. *J. Appl. Phys.* **2002**, *91*, 2959. (d) Dorenbos, P. *Phys. Status Solidi B* **2005**, *242*, R7. (e) Takasaki, H.; Tanabe, S.; Hanada, T. *J. Ceram. Soc. Jpn.* **1996**, *104*, 322. (f) Akiyama, M.; Xu, C. N.; Nonaka, K.; Watanabe, T. *Appl. Phys. Lett.* **1998**, *73*, 3046.
(24) (a) Abbruscato, V. *J. Electronchem. Soc.* **1971**, *118*, 930. (b) Wang, Z. Y.; Wang, Y. H.; Zhang, P. Y.; Fan, X. P.; Qian, G. D. *J. Lumin.* **2007**, *124*, 140.
(25) Hosono, H.; Kinoshita, T.; Kawazoe, H.; Yamazaki, M.; Yamamoto, Y.; Sawanobori, N. *J. Phys.: Condens. Matter.* **1998**, *10*, 9541.
(26) Fu, J. *Electrochem. Solid-State Lett.* **2000**, *3*, 350.
(27) Blasse, G.; Bril, A. *Philips Res. Rep.* **1966**, *2*, 368.
(28) (a) Shen, W. Y.; Pang, M. L.; Lin, J.; Fang, J. Y. *J. Electrochem. Soc.* **2005**, *152*, H25. (b) Fujii, T.; Kodaira, K.; Kawauchi, O.; Tanaka, N.; Yamashita, H.; Anpo, M. *J. Phys. Chem. B* **1997**, *101*, 10631.

$$\langle\tau\rangle = (A_1^2\tau_1^2 + A_2^2\tau_2^2)/(A_1\tau_1 + A_1\tau_1) \quad (5)$$

can be determined to be 0.372 and 0.600 ms for samples 1 and 2, respectively. The lifetime of sample 2 is basically somewhat longer than that of 0.41 ms reported for Eu^{3+} in $ZnWO_4$nanocrystals,[30] but shorter than that of 0.74 ms for YVO_4:Eu^{3+} nanocrystals[31] and that of 0.65 ms for YVO_4:Eu^{3+}/SiO_2 core/shell materials.[1e] On the basis of emission spectra and the lifetimes of $^5D_0$ emitting level, the quantum efficiency, η, of $^5D_0$ for Eu^{3+} ions in $CaWO_4$ nanocrystals can be determined. Assuming that only nonradiative and radiative processes are involved in the depopulation of the $^5D_0$ level, the quantum efficiency can be expressed as

$$\eta = A_{rad}/(A_{rad} + A_{nrad}) \quad (6)$$

where the parameters A_{rad} and A_{nrad} denote the radiative and nonradiative transition rates. The A_{rad} for $^5D_0$ state was obtained as described next. First, the emission intensity, I, taken as the integral intensity S of the $^5D_0$—$^7F_{0-4}$ emission lines, was defined as

$$I_{i-j} = \tilde{\hbar}\omega_{i-j}A_{i-j}N_i \approx S_{i-j} \quad (7)$$

where i and j are the initial level $^5D_0$ and the final levels $^7F_{0-4}$, respectively, while $\tilde{\hbar}\omega_{i-j}$ is the transition energy, A_{i-j} is the Einstein's coefficient of spontaneous emission, and N_i is the population of the $^5D_0$ level. Since no transitions related to $^5D_0$—$^7F_5$ and $^5D_0$—$^7F_6$ were experimentally detected, the influences of these transitions on the depopulation of $^5D_0$ excited level were neglected.[32] Considering the character of the magnetic dipole transition ($^5D_0$—$^7F_1$) and its weak dependence on the crystal field effect, the $A_{0\text{-}1}$ coefficient was used as a reference for the complete spectrum. The experimental coefficients of spontaneous emission were then calculated according to the equation

$$A_{0J} = A_{01}(I_{0J}/I_{01})(\nu_{01}/\nu_{0J}) \quad (8)$$

where ν_{01} and ν_{0J} are the energy baricenters of the $^5D_0$—$^7F_1$ and $^5D_0$—^7F_J transitions, respectively. A_{01} is the Einstein's coefficient of spontaneous emission between $^5D_0$ and $^7F_1$ levels. In vacuum, $(A_{0\text{-}1})_{vac}$[33] is assumed to be 14.65 s^{-1}. The value of $A_{0\text{-}1}$ was expressed as,

$$A_{0-1} \approx n^3(A_{0-1})_{vac} \quad (9)$$

where n indicates the average refractive index of $CaWO_4$ nanocrystals. It is known that the average refractive index in nanoscale materials is different from that in bulk materials. Previous studies[34] investigated the temperature dependence of refractive index and volume expansion coefficient of lead molybdate and found that the temperature derivation of the refractive index and volume expansion coefficient could be denoted as $\partial\ln n/\partial T = -30n_0 \times 10^{-6}$/K and $\partial\ln v/\partial T = -161 \times 10^{-6}$/K (longitudinal wave along c axis), respectively. $CaWO_4$ has a closely structural link to $PbMoO_4$. Therefore, it is reasonable to assume that the temperature dependence of refractive index and volume expansion coefficient of $CaWO_4$ is similar to that of $PbMoO_4$. Here, the lattice volumes of $CaWO_4$ nanocrystals were determined to be 317.9 and 315.8 $Å^3$ for samples 1 and 2, respectively, which are a little larger than 312.5 $Å^3$ of bulk $CaWO_4$. Combined with the temperature dependence of lattice volume of $CaWO_4$[35] and the refractive index (n_0 = 1.97) of bulk $CaWO_4$ according to Wahl et al.,[36] the average refractive index of $CaWO_4$ nanocrystals can be estimated as 1.92 and 1.94 for samples 1 and 2, respectively. Consequently, $A_{0\text{-}1}$ is estimated to be 109 s^{-1} for sample 1 and 110 s^{-1} for sample 2. Finally, A_{rad} is obtained by summing over the radiative rates A_{0J} for each $^5D_0$—^7F_J transition. Because lifetime (τ), radiative, and nonradiative transition rates have the following relationship

$$A_{tot} = \frac{1}{\tau} = A_{rad} + A_{nrad} \quad (10)$$

A_{nrad} can be obtained after determining the values of τ and A_{rad}. By using eq 6, the quantum efficiencies for samples 1 and 2 were calculated to be 28.6 and 54.9%, respectively. It is clear that the quantum efficiency of sample 2 is much higher than that of sample 1, which seems to be consistent with the longer lifetime of sample 2. The enhanced quantum efficiency and the increased lifetime for sample 2 could be interpreted as a decrease in nonradiative combination centers, the codoping of Na^+ and Eu^{3+}, and lattice expansion at smaller sizes as well. Nonradiative combination centers can be produced by many factors, such as defects and surface states. As the particle size reduces to nanoscale regime, the size effects and surface chemistry are usually the main factors. Considering the size effects of $CaWO_4$:Eu^{3+}/Na^+ nanocrystals, the low temperature synthesis and small particle size for present $CaWO_4$:Eu^{3+}/Na^+ nanocrystals probably lead to numerous bulk and surface defects in the samples, in which some defects may serve as the nonradiative recombination centers for the decreased quantum efficiency. Sample 1 has a relatively small particle size of only 5 nm, and as a result, much more nonradiative recombination centers would be expected to exist that reduce the quantum efficiency of $^5D_0$ for Eu^{3+}. With regards to the effect of nonradiative recombination centers, the surface states have to be considered. As is for the nanocrystals prepared by wet chemical methods, the surfaces of the particles are covered by a great number of OH groups either chemically bonded or physically adsorbed on the surfaces, as indicated by our previous work[13b] and IR spectra for the present samples (see the Supporting Information, Figure S4). These hydroxyl groups can be the very efficient quenchers of the lumines-

(29) (a) Bauer, R. K.; Borenstein, R.; Mayo, P. de; Okada, K.; Rafalska, M.; Ware, W. R.; Wu, K. C. *J. Am. Chem. Soc.* **1982**, *104*, 4635. (b) Bauer, R. K.; Mayo, P. de; Ware, W. R.; Wu, K. C. *J. Phys. Chem.* **1982**, *86*, 3781.
(30) Dai, Q. L.; Song, H. W.; Bai, X.; Pan, G. H.; Lu, S. Z.; Wang, T.; Ren, X. G.; Zhao, H. F. *J. Phys. Chem. C* **2007**, *111*, 7586.
(31) Riwotzki, K.; Haase, M. *J. Phys. Chem. B* **2001**, *105*, 12709.
(32) (a) Soares-Santos, P. C. R.; Nogueira, H. I. S.; Fe'lix, V.; Drew, M. G. B.; Sa' Ferreira, R. A.; Carlos, L. D.; Trindade, T. *Chem. Mater.* **2003**, *15*, 100. (b) Sa' Ferreira, R. A.; Carlos, L. D.; Goncüalves, R. R.; Ribeiro, S. J. L.; de Zea Bermudez, V. *Chem. Mater.* **2001**, *13*, 2991. (c) Carlos, L. D.; Messaddeq, Y.; Brito, H. F.; Sa' Ferreira, R. A.; de Zea Bermudez, V.; Ribeiro, S. J. L. *Adv. Mater.* **2000**, *12*, 594.
(33) Peng, C. Y.; Zhang, H. j.; Yu, J. B.; Meng, Q. G.; Fu, L. S.; Li, H. R.; Sun, L. N.; Guo, X. M *J. Phys. Chem. B* **2005**, *109*, 15278.
(34) (a) Coquin, G. A.; Pinnow, D. A.; Warner, A. W. *J. Appl. Phys.* **1971**, *42*, 2162. (b) Sonehara, T.; Tatsu, E.; Saikan, S. *J. Appl. Phys.* **2007**, *101*, 103507.
(35) Achary, S. N.; Patwe, S. J.; Mathews, M. D.; Tyagi, A. K. *J. Phys. Chem. Solids* **2006**, *67*, 774.
(36) Wahl, D.; Mikhailik, V. B.; Kraus, H. *Nucl. Instrum. Methods Phys. Res., Sect. A* **2007**, *570*, 529.

cence of lanthanide elements through multiphonon relaxation.[37] Huignard and co-workers[38] demonstrated that the transfer of YVO_4:Eu^{3+} colloidal from water to deuterated water reduces the multiphonon relaxation and thus enhances the luminescent efficiency. Moon et al.[39] have systematically studied the hydroxyl groups on the quenching of luminescence efficiencies in SnO_2:Eu^{3+} nanocrystals. In our previous work, we have found that the sample prepared at room temperature has much more surface OH groups than that obtained after hydrothermal treatments.[13b] Therefore, the hydroxyl quenching effect would be suppressed in sample 2. Furthermore, the codoping of Eu^{3+} and Na^+ at Ca^{2+} sites in sample 2 also plays a very important role in the enhanced quantum efficiency. Numerous papers have reported that the addition of alkali metal ions into the rare-earth-doped materials results in a significant enhancement of the luminescence properties,[40] which is all based on the modifications of the local symmetry and the surroundings near the rare earth ions by the addition of coactive ions or charge compensators of alkali metal ions.[40b,c,41] For the present work, when Na^+ ions were incorporated into $CaWO_4$ lattice in/near $Eu-O_8$ cluster to maintain a local charge balance between Eu^{3+} and Na^+, the structure of the $Eu-O_8$ would not be destroyed but a slight structural modification and the resulting lowered symmetry of the crystal field around Eu^{3+}. The wave functions of Eu^{3+} ions have a tendency to mix to some extent with those of the neighboring O^{2-} and Na^+ ions as that in the Er^{3+}/Li^+ codoped ZnO powders.[41] Because the Na^+ concentration in sample 2 is higher than that of sample 1 (Table 1), an increased number of the distorted $Eu-O_8$ with optically active centers is expected. This reasoning seems to be consistent with XRD analysis. As stated above, sample 1 showed a lattice expansion which is followed by a decreased axial ratio of *c*/*a* in comparison with sample 2. The *c*/*a* value tending to 2 corresponded to the ideal structure of equal cation coordination.[42] Consequently, the increase of *c*/*a* value indicated the enhanced asymmetry ratio, which agrees with the ratios of structural hypersensitive R/O (intensity ratio of transition $^5D_0-^7F_2$ to $^5D_0-^7F_1$).[43] The reduction of lattice symmetry would result in much distorted $Eu-O_8$ clusters and enhance the luminescent intensity.

To demonstrate efficient incorporation of the Eu^{3+} and Na^+ ions in $CaWO_4$ host matrix, a series of $Ca_{1-2x}(Eu,Na)_{2x}WO_4$ nanocrystals were also prepared at 160 °C by varying the initial molar ratios of the hydrothermal conditions. Typical XRD patterns in Figure 5 indicated that all samples crystallized in a pure tetragonal phase of $CaWO_4$ with increasing the dopant content up to $x = 0.135$. The structural refinements of XRD data for $Ca_{1-2x}(Eu,Na)_{2x}WO_4$ nanocrystals (inset of Figure 5) show that for $x \leq 0.122$, the cell volume increased linearly with x. When the Eu^{3+} concentration was increased beyond $x = 0.122$, the cell volume did not have apparent changes, which implied that the solubility of Eu^{3+} ions in $CaWO_4$ nanocrystals was about 12.2%. As discussed above, Eu^{3+} prefers locating at Ca^{2+} site because of the similar ionic radii, whereas Na^+ ions could be simultaneously introduced into $CaWO_4$ host matrix to maintain the charge balance. The Eu content dependence of the cell volume (inset of Figure 5) follows this trend.

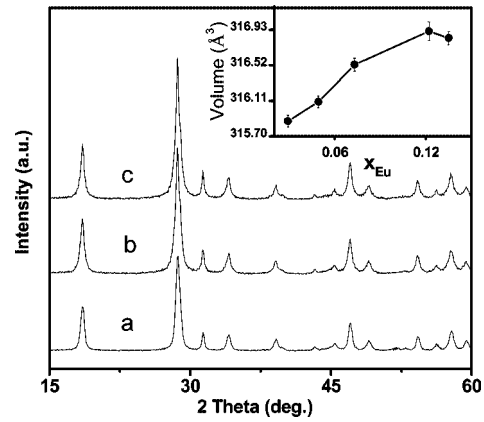

Figure 5. XRD patterns of the samples $Ca_{1-2x}(Eu,Na)_{2x}WO_4$ at (a) $x_{Eu} = 0.029$, (b), $x_{Eu} = 0.073$, and (c) $x_{Eu} = 0.135$ prepared by under hydrothermal condition at 160 °C. Inset shows the evolution of the unit cell volume versus the Eu^{3+} fraction.

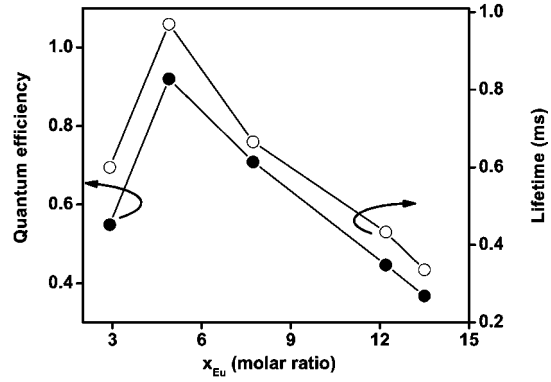

Figure 6. Quantum efficiencies and lifetimes as a function of Eu^{3+} content in $Ca_{1-2x}(Eu,Na)_{2x}WO_4$ nanocrystals.

Figure 6 presents the quantum efficiencies as a function of Eu^{3+} doping concentration for the $Ca_{1-2x}(Eu,Na)_{2x}WO_4$ nanocrystals. It is clear that the quantum efficiency increased with Eu^{3+} concentration to show a maximum of about 92% at $x = 0.049$, whereas further increasing the Eu^{3+} concentration led to a significant decrease in the quantum efficiency. The optimal concentration of Eu^{3+} is smaller than $x = 0.3$ reported for $CaWO_4$:Eu^{3+} incorporated in silica[9c] and $CaWO_4$:Eu^{3+} film.[6c] As for the bulk luminescence materials, the presence of the maximum quantum efficiency is a consequence of the competition between the number of luminescence centers and the concentration quenching effect. As the content of rare earth ions increases, the excited-state of luminescence centers can be transferred resonantly through the system and a trap can be reached very easily, which means that the possibility of a nonradiative de-excitation via a luminescence killer is increased. As a consequence, the

(37) Blasse, G. *Prog. Solid State Chem.* **1988**, *18*, 119.
(38) Huignard, A.; Gacoin, T.; Boilot, J. P. *Chem. Mater.* **2000**, *12*, 1090.
(39) Moon, T.; Hwang, S. T.; Jung, D. R.; Son, D.; Kim, C.; Kim, J.; Kang, M.; Park, B. *J. Phys. Chem. C* **2007**, *111*, 4164.
(40) (a) Lopez, O. A.; Mckittrick, J.; Shea, L. E. *J. Lumin.* **1997**, *71*, 1. (b) Gu, F.; Wang, S. F.; Lu, M. K.; Zhou, G. J.; Xu, D.; Yuan, D. R. *Langmuir* **2004**, *20*, 3528. (c) Pang, M. L.; Shen, W. Y.; Lin, J. *J. Appl. Phys.* **2005**, *97*, 033511.
(41) Zhou, Z.; Komori, T.; Ayukawa, T.; Yukawa, H.; Morinaga, M. *Appl. Phys. Lett.* **2005**, *87*, 091109.
(42) Errandonea, D.; Manjón, F. J.; Somayazulu, M.; Häusermann, D. *J. Solid State Chem.* **2004**, *177*, 1087.
(43) Shi, S. K.; Liu, X. R.; Gao, J.; Zhou, J. *Spectrochim. Acta, Part A* **2008**, *69*, 396.

decay time becomes shorter. The lifetimes of $CaWO_4:Eu^{3+}/Na^+$ nanocrystals as a function of Eu^{3+} doping concentration are shown in Figure 6. It is seen that the composition with 4.90% Eu^{3+} content possess the longest lifetime of 0.969 ms. When Eu^{3+} content was increased to 13.5%, the luminescence decay time was shortened to 0.336 ms. Surprisingly, the quantum efficiency and lifetime of $Ca_{1-2x}(Eu^{3+},Na^+)_{2x}WO_4$ nanocrystals showed the same variation trend with Eu content. Similar optimum concentration of rare earth luminescence ions has also been observed for Er^{3+} doped $Bi_2O_3-B_2O_3-SiO_2$ glasses[44] and Eu^{3+}-doped ZrO_2 and Y_2O_3 systems imbedded in silica.[45] The highest quantum efficiency of $CaWO_4:Eu^{3+}/Na^+$ nanocrystals here is much higher than 68% of $La_2(WO_4)_3:Eu^{3+}$ prepared by a two step Pechini method[9a] and 59% of $LaPO_4:Eu^{3+}$ nanowires fabricated by a hydrothermal treatment,[46] but still lower than some commercial phosphors, such as $Y_2O_3:Eu^{3+}$ with quantum efficiency of nearly 100%.[2a] The high quantum efficiencies suggest that $Ca_{1-2x}(Eu,Na)_{2x}WO_4$ nanocrystals can be a promising red phosphor.

Conclusions

Scheelite nanostructures $Ca_{1-2x}(Eu,Na)_{2x}WO_4$ ($0 < x \leq 0.135$) were prepared by hydrothermal treatment of nanocrystals synthesized at room temperature. The sample prepared at room temperature was 5 nm $Ca_{0.968}(Eu,Na)_{0.032}WO_4$, which had a quantum efficiency of 28.6%. Upon subsequent hydrothermal treatments, Eu^{3+} and Na^+ concentrations in the scheelite nanostructures increased and significantly enhanced the quantum efficiency. One notable result of this work is the demonstration that chemical compositions can be controlled to tune the local symmetry surrounding Eu^{3+} and moreover the energy transfer from O^{2-} to Eu^{3+} and tungstate groups to Eu^{3+} to have excellent luminescence properties as featured by luminescence lifetimes of milliseconds, abnormally narrowed emissions, and maximum quantum efficiencies as high as 92%.

Acknowledgment. This work was financially supported by NSFC (Contracts 20671092, 20773132, 20771101), National Basic Research Program of China (973 Program, 2009CB939801, 2007CB613306), and Directional program CAS (KJCXZ-YW-M05) and FJIRSM (SZD-07004-3). The authors express their sincere thanks to Professor Richard Lee Smith, Jr. (Tohoku University, Japan), for reading the revised manuscript and for many important discussions as part of our ongoing collaboration.

Supporting Information Available: XRD patterns; excitation, luminescence, and IR spectra (PDF). This material is available free of charge via the Internet at http://pubs.acs.org.

CM8014435

(44) Dai, S. X.; Xu, T. F.; Nie, Q. H.; Shen, X.; Wang, X. S. *Phys. Lett. A* **2006**, *359*, 330.
(45) Riello, P.; Bucella, S.; Brunelli, D.; Fossa, F.; Benedetti, A.; Trave, E.; Mazzoldi, P. *Opt. Mater.* **2006**, *28*, 1261.
(46) Yu, L. X.; Song, H. W.; Lu, S. Z.; Liu, Z. X.; Yang, L. M.; Kong, X. G. *J. Phys. Chem. B* **2004**, *108*, 16697.